Iran J. Earth Sci. 2026; 18(3): 366-382

Iranian Journal of Earth Sciences (IJES)

https://doi.org/10.57647/j.ijes.2025.16951

Research Article

Application of Ti-in-Quartz and Zr-in-Rutile Thermometers to Constrain Pressure-Temperature in Meta-Ophiolitic Rocks of the Kazdağ Massif, NW Anatolia

Firat Şengün

Department of Mining and Mineral Extraction, Çan Vocational College, Çanakkale Onsekiz Mart University, 17400, Çan-Çanakkale, Turkey

***Corresponding author:** firatsengun@comu.edu.tr

Article History:

Received:
15 August 2024

Revised:
3 November 2024

Accepted:
1 February 2025

Published Online:
25 June 2025

Published in Issue:
30 September 2026

Abstract

Ophiolitic metagabbros are exposed in the Kazdağ Massif located in the northwestern part of Anatolia. Trace element compositions in rutile and quartz were determined for metagabbros from the Kazdağ Massif by LA-ICP-MS. Ti-in-quartz can be used as a thermobarometer in combination with the Zr-in-rutile thermometer. P-T conditions for ophiolitic metagabbros were calculated from the Ti content of quartz and Zr content of rutile, which are in equilibrium with each other. Ti contents of quartz ranged between 28 and 42 µg/g (average 36 µg/g). A P–T estimate can be obtained from the intersection of the Ti-in-quartz isopleths with the Zr-in-rutile isopleths, which yield ~ 660 ℃ and 1 GPa under amphibolite-facies conditions. The P-T conditions of meta-ophiolitic rocks suggest that they formed as a separate higher-pressure tectonic slice in the Kazdağ Massif. Amphibolite-facies metamorphism resulted from northward subduction of the İzmir-Ankara branch of the Neo-Tethyan Ocean under the Sakarya Zone. Metamorphism was followed by internal imbrication of the Kazdağ Massif, resulting from southerly directed compression during internal collision. Later, the Sakarya Zone collided with the Anatolide-Tauride Block located in the south. This collision and internal imbrication of the Kazdağ Massif caused thickness in the crust.

Keyword: Metamorphism; Rutile; Quartz; Thermobarometer; Metagabbro; NW Anatolia

Cite this article: Şengün, F. (2026). Application of Ti-in-Quartz and Zr-in-Rutile Thermometers to Constrain Pressure-Temperature in Meta-ophiolitic Rocks of the Kazdağ Massif, NW Anatolia. *Iranian Journal of Earth Sciences*, *18*(3), 366–382. https://doi.org/10.57647/j.ijes.2025.16951

1. Introduction

Quartz is a common mineral in igneous, metamorphic, hydrothermal and sedimentary rocks, which attests to its stability over a wide range of P-T conditions. Trace element geochemistry of quartz provides significant information about the crystallization conditions of rocks. During the co-crystallization of rutile (TiO_2) and quartz, Ti^{4+} substitutes for Si^{4+} on the tetrahedral side in quartz, which highly depends on temperature and pressure (Wark and Watson, 2006). Therefore, the solubility of Ti in quartz has been calibrated experimentally, resulting in the Ti-in-quartz (TitaniQ) thermobarometer, and can be used to obtain P-T estimates for crystallization. The P–T dependence of Ti-in-quartz solubility can be used as a geothermobarometer in combination with another thermobarometer in a coexisting mineral (e.g., Zr-in-rutile thermometer) or an independent P or T estimate for quartz crystallization (Thomas et al., 2010; 2015; Yazdi et al. 2017; Mollai et al. 2021; Nazari et al. 2023; Ashrafi et al. 2024). Similarly, zirconium incorporation into the crystal lattice of rutile is strongly dependent on temperature in quartz- and zircon-bearing systems, which allowed the development of Zr-in-rutile thermometers (Zack et al., 2004; Watson et al., 2006; Ferry and Watson, 2007; Tomkins et al., 2007; Salehpour et al. 2025; Borojenie et al., 2025) Ti-in-quartz and Zr-in-rutile thermometers are powerful single-mineral thermometers and have been widely applied to constrain metamorphic temperatures of medium- to high-grade and ultra high-grade metamorphic rocks (Zack and Luvizotto, 2006; Zhang et al., 2009; Meyer et al., 2011; Ewing et al., 2013; Gao et al., 2014).

Rutile (TiO_2) is an important accessory mineral that commonly occurs in high-grade metamorphic rocks from oceanic and continental subduction zones (e.g., Foley et al., 2002; Zack et al., 2002; Meinhold, 2010; Ding et al., 2013). Rutile is a major titanium-bearing phase that carries high field strength elements (HFSE) and dominates the Nb, Ta and Ti budgets of many rocks in subduction zone systems (Brenan et al., 1994; Green, 1995; Foley et al., 2000; Rudnick et al., 2000). It can also accommodate a wide range of highly-charged trace elements up to the percent level, such as V, Cr, Fe, Al, Sn, Sb and W (e.g., Graham and Morris, 1973; Deer et al., 1992; Zack et al., 2002).

The metamorphic sequence of the Kazdağ Massif has been previously described as a metamorphic complex consisting of various gneisses, amphibolites, marbles and meta-ophiolites (Okay et al., 1996; Duru et al., 2004; Okay et al., 2006). However, the internal succession, contact relations of various rock types, and origin of assembly remain under debate. The main questions regarding the metamorphic evolution and tectonic setting of the meta-ophiolites also remain unanswered.

The Ti-in-quartz (TitaniQ) thermometer has been applied to calculate the P-T conditions of metagabbros widely occurring in meta-ophiolitic rocks. Fe-Mg exchange, Zr-in-rutile thermometers and Grt-Hbl-Pl-Qz geothermobarometer were applied to estimate metamorphic P-T conditions of meta-ophiolitic rocks (Okay and Satır, 2000; Şengün and Zack, 2016).

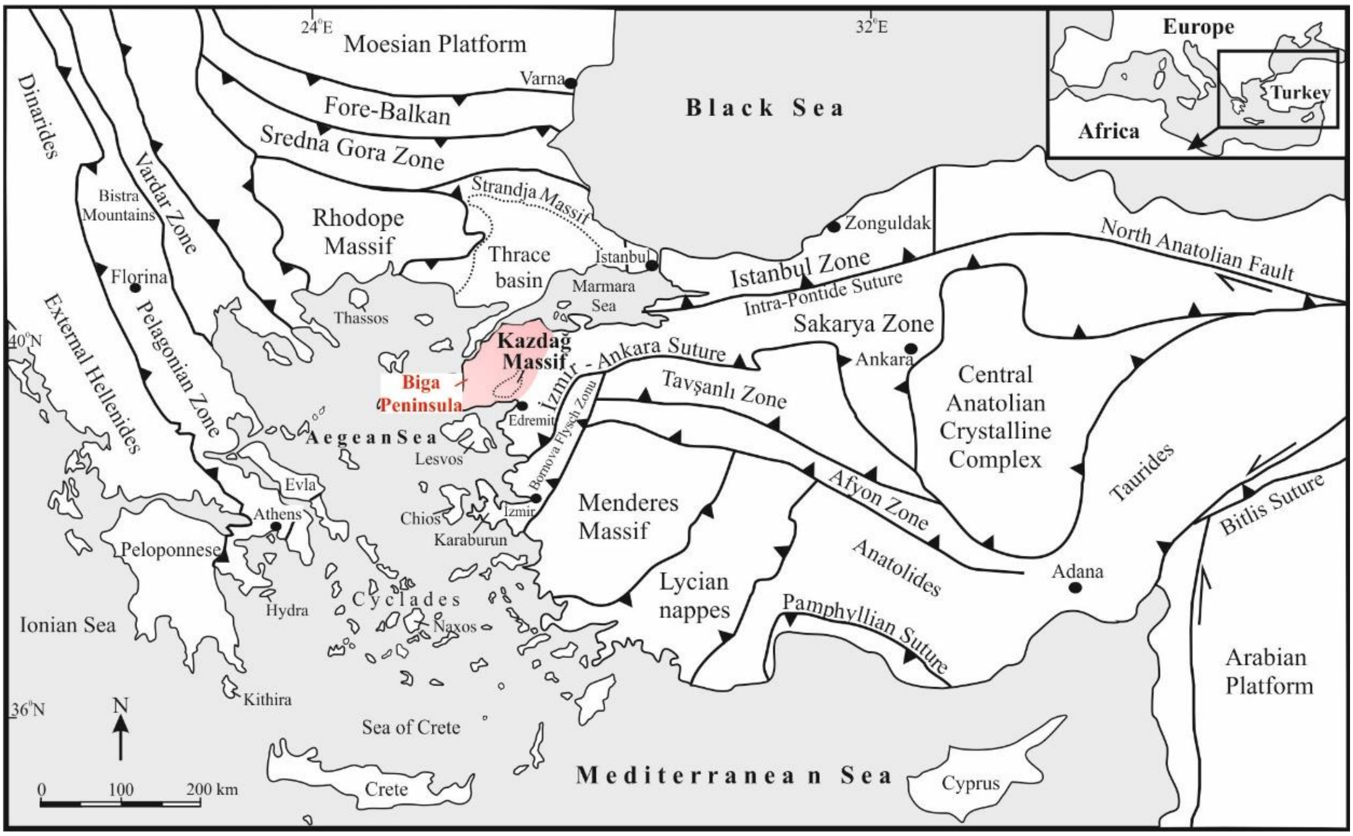

Figure 1. Tectonic map of the Eastern Mediterranean region indicating major geotectonic units and bounding sutures (modified from Okay et al., 1996; Meinhold et al., 2010)

10.57647/j.ijes.2025.16951

The Ti-in-quartz thermometer was examined to check how well it fits with conventional thermometers, with the aim of assessing how reliable this thermometer is for subduction systems. Rutile geochemistry combined with Zr-in-rutile and Ti-in-quartz thermometers can allow evaluation of the trace element behaviours of subducted oceanic crust and metamorphic evolution in subduction zone processes. The aim of this study is to apply the Ti-in-quartz thermobarometer to constrain pressure and temperature conditions of metagabbros from the Kazdağ Massif (NW Anatolia) and to provide insights into the metamorphic evolution of subducted oceanic crust from the rutile chemistry in high-grade metamorphic rocks.

2. Geological Setting

Türkiye is commonly subdivided into several tectonic terrains separated by ophiolitic suture zones, representing the closure of branches of Tethyan ocean basins during the Mesozoic and Cenozoic (Fig. 1) (e.g., Şengör and Yılmaz, 1981; Okay and Tüysüz, 1999; Moix et al., 2008). These are, from north to south, the Sakarya Zone (Okay, 1984), the İzmir-Ankara Zone (Şengör and Yılmaz, 1981), the Tavşanlı Zone (Okay, 1986), the Afyon Zone (Okay, 1984), and the Menderes Massif (Dürr et al., 1978).

Anatolia is situated at the intersection of the Africa and Eurasian plates, and has been assembled through numerous subduction and collisional events since the Early Mesozoic. Northwestern Anatolia is known as region where different tectonic units meet and forms one of the critical regions in the geology of Türkiye (e.g., Okay and Satır, 2000; Beccaletto and Jenny, 2004; Şengün et al., 2011; Aysal et al., 2012; Okay and Topuz, 2017; Karslı et al., 2020; Topuz et al., 2020). The Sakarya Zone, one of these crustal units, is an E-W–trending continental sliver bordered by the İstanbul Zone, the Thrace Basin in the north, and the Bornova Zone and Tavşanlı Zone in the south (Fig. 1). The Kazdağ Massif lies in the Sakarya Zone and is located in the south of the Biga Peninsula (Fig. 2). The Kazdağ Massif structurally forms a NE-SW–plunging anticlinorium of medium to high-grade metamorphic rocks representing the deepest section of continental crust exposed in north-west Anatolia (Bingöl, 1969; Okay et al., 1991; Okay and Satır, 2000; Duru et al., 2004). The Kazdağ Massif is generally regarded as a latest Oligocene metamorphic core complex (Okay et al., 1991; Okay and Satır, 2000). The medium-grade metamorphic basement rocks of the Kazdağ Massif are mainly composed of felsic gneisses, amphibolite, marble and meta-ophiolitic rocks at the basal – middle part of the massif, and meta-granite associated migmatite, amphibolite, and marble intercalations at the top (Fig. 3) (e.g., Okay and Satır, 2000; Duru et al., 2004; Erdoğan et al., 2013; Yiğitbaş et al., 2014).

The meta-ophiolitic rocks of the Kazdağ Massif occur in the core of the anticlinorium enveloped by a marble-rich sequence, which passes up to felsic gneisses with migmatite,

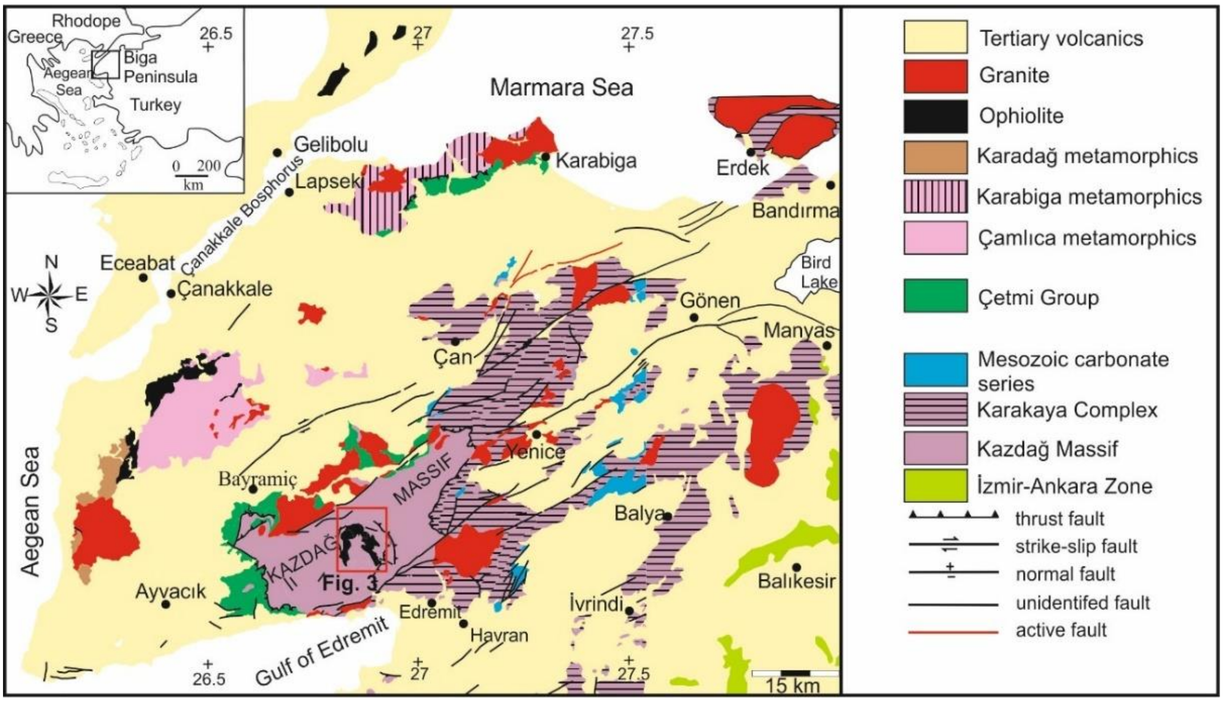

Figure 2. Generalized geological map of the Biga Peninsula (modified from MTA, 2012)

10.57647/j.ijes.2025.16951

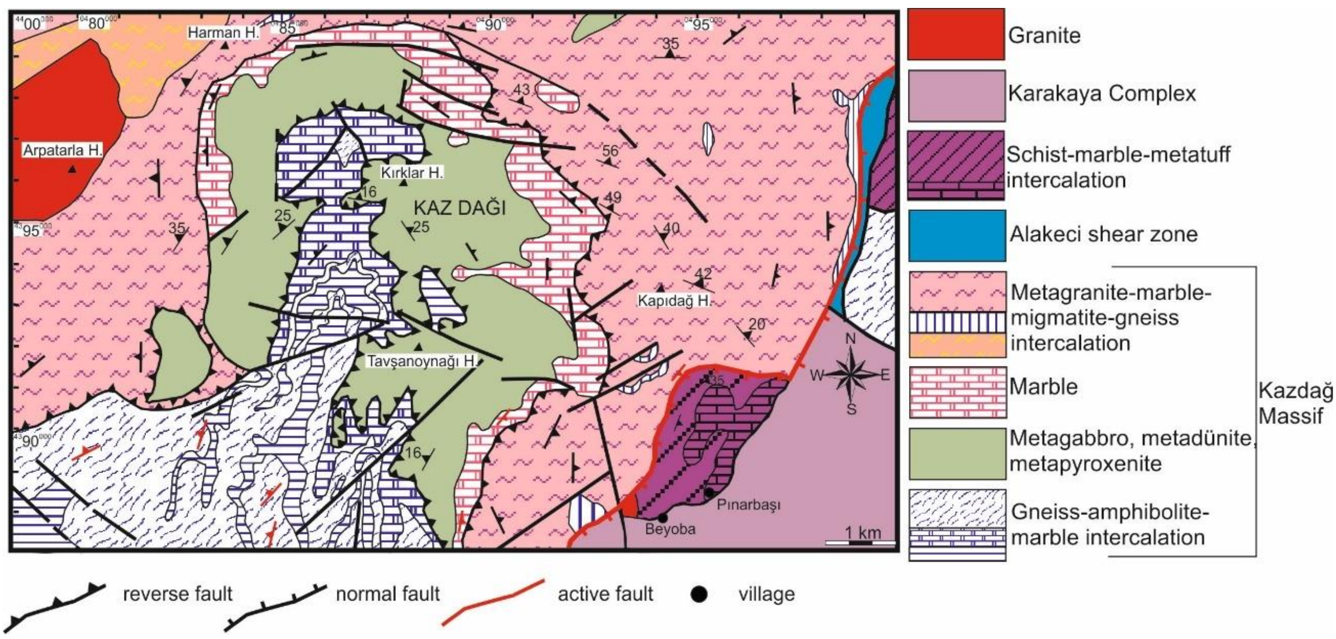

Figure 3. Detailed geological map of meta-ophiolitic rocks in the Kazdağ Massif (modified from Duru et al., 2004)

marble and amphibolite (Bingöl, 1969; Okay and Satır, 2000; Duru et al., 2004; Erdoğan et al., 2013; Şengün et al., 2023). The Kazdağ Massif is subdivided into four formations (Duru et al., 2004; Fig. 3). These are, from the base to the top, (i) the Fındıklı Formation consists of an intercalation of amphibole-bearing gneiss, quartz-feldspathic gneiss, marble, and amphibolite. (ii) The Tozlu meta-ophiolite is mainly composed of meta-ophiolitic rocks including metagabbro, meta-pyroxenite, meta-dunite, and serpentinite. (iii) The Sarıkız unit consists of platform-type, highly recrystallized white marbles with gneiss horizons. (iv) The Sütüven Formation forms the uppermost part of the Kazdağ Massif and comprises quartz-feldspathic gneisses with a lesser amount of amphibolite and marble horizons and lenses. Moreover, migmatization is widely observed in the quartz-feldspathic gneisses of the Sütüven Formation. The Sütüven Formation is intruded by Oligo-Miocene granodiorite.

The metamorphic rocks of the Kazdağ Massif underwent amphibolite- to granulite-facies metamorphism under progressive compression during the Alpine orogeny, associated with the emplacement of meta-granites (Okay and Satır, 2000; Erdoğan et al., 2013). Zircon ages from felsic gneisses and amphibolite in the Kazdağ Massif were 308±16 Ma and 329±5 Ma, respectively, determined by the single-zircon stepwise Pb evaporation method (Okay and Satır, 2000). However, K-Ar mica ages from two gneisses in the Kazdağ Massif yielded 26±3 Ma and 27±3 Ma, which are related to the Alpine overprint (Bingöl, 1969). More recently, U-Pb zircon ages from meta-granite samples yielded 24.8±4.6 Ma and 28±10 Ma, which is interpreted to represent migmatitic metamorphism in the Kazdağ Massif occurring during the Alpine orogeny (Erdoğan et al., 2013). This isotopic data suggests that medium-grade metamorphism in the Kazdağ Massif occurred during the Carboniferous and during the late Oligocene (Okay et al., 1996; Okay and Satır, 2000; Erdoğan et al., 2013; Yiğitbaş et al., 2014). Apatite fission-track ages of 17-14 Ma from the Alakeçi shear zone located on the western flank of the Kazdağ Massif were linked to exhumation of the Kazdağ Massif (Cavazza et al., 2009).

The medium-grade metamorphic rocks of the Kazdağ Massif are tectonically overlain by the Permo-Triassic Karakaya Complex (Bingöl et al., 1975), comprising low-grade meta-morphic and sedimentary rocks, subduction-accretionary intra-oceanic arc/forearc units, marking the closure of the Palaeotethyan oceanic domain (Okay et al., 1996; Okay and Göncüoğlu, 2004).

3. Petrography

The studied samples were taken from metagabbros (1130, 1301) and amphibolites (1184, 1202) in the meta-ophiolitic rocks. Metagabbro is the dominant rock type that includes rutile minerals. Metagabbro occurs as layers of varying thickness, which alternate with amphibolite and meta-dunite. Metagabbro is black-coloured, coarse-grained (0.5 to 0.8 mm), well foliated and banded (Fig. 4a). These layers of amphibolite have alternating plagioclase and amphibole-rich bands (Fig. 4b). The main mineral assemblage of metagabbro is dominated by

10.57647/j.ijes.2025.16951

plagioclase (~40 vol. %), hornblende (~30 vol. %), clinopyroxene (~15 vol. %), orthopyroxene (~5 vol. %), and biotite (~5 vol. %) (Fig. 4c, d). The most conspicuous textures in the metagabbros are grano-nematoblastic and poikiloblastic. Plagioclase is very common, medium to coarse, lath-shaped and exhibits polysynthetic twinning. Hornblende is coarse-grained, with pleochroism of colorless to light green and green to greenish-brown. Clinopyroxene is more abundant (~15 vol. %) and occurs as medium to coarse subhedral grains frequently replaced by epidote and hornblende. Orthopyroxene has limited abundance (~10 vol. %) and is pleochroic from pale pink to pale green. Accessory mineral phases include epidote, chlorite, quartz, rutile, titanite, zircon, apatite and ilmenite. Inclusion of quartz, epidote and zircon occurs in clinopyroxene minerals.

Hornblende (~50 vol. %), plagioclase (~35 vol. %), quartz (~5 vol. %), biotite (~5 vol. %), and garnet (~5 vol. %) represent the main mineral assemblage in the amphibolites (Fig. 4e, f). Accessory and secondary mineral phases are mainly composed of epidote, chlorite, biotite, titanite, zircon, apatite, and ilmenite. Hornblende forms the dominant mafic mineral phase in amphibolites and has subhedral crystal form (Fig. 4e). Prismatic to elongated hornblende crystals are intergrown with later mineral phases.

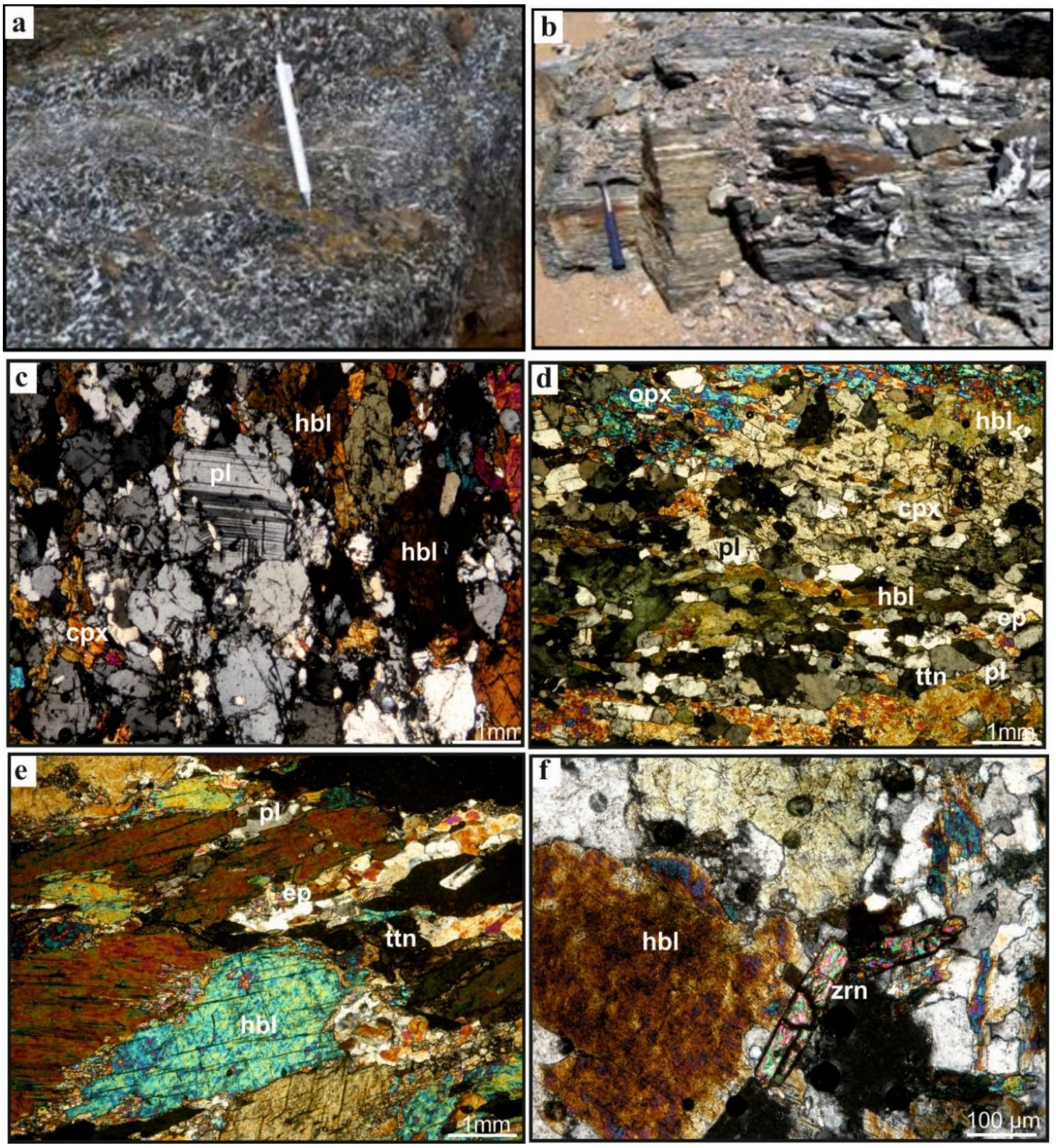

Figure 4. (a) General view of black-coloured, coarse-grained metagabbro, (b) banded amphibolite, (c) texture of metagabbro, (d) amphibolite represented by elongated hornblende and plagioclase grains, (e) prismatic to elongated hornblende crystals in amphibolite, (f) accessory zircon crystals occur in metagabbro (hbl: hornblende, cpx: clinopyroxene, opx: orthopyroxene, pl: plagioclase, zrn: zircon, ttn: titanite, ep: epidote, mineral abbreviations are from Warr, 2021)

10.57647/j.ijes.2025.16951

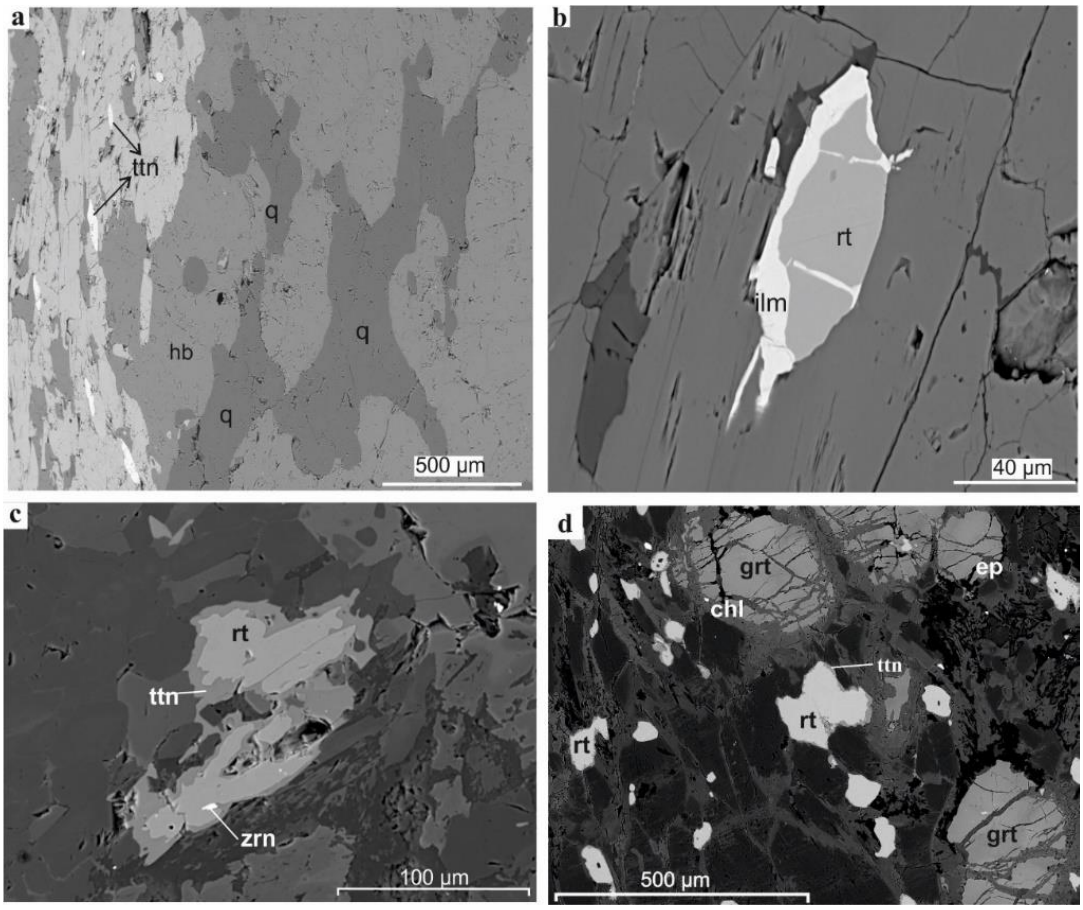

Figure 5. Back scattered electron (BSE) images (sample 1202) showing the textural relationships, (a) quartz (q) grains occurring in the matrix, (b) rutile surrounded by ilmenite (ilm) rim, (c) rutile grains are mantled by titanite, (d) pseudomorphic replacement of garnet by chlorite-epidote assemblage (rt: rutile, ttn: titanite, grt: garnet, chl: chlorite, ep: epidote, il: ilmenite, zrn: zircon)

Gray to yellow-coloured, anhedral quartz grains occur as inclusions in both the matrix and hornblende (Fig. 5a). Quartz grains in the matrix are 200-350 µm in size. However, the size of quartz inclusions varies from 30 µm to 50 µm. Rutile grains occur either as 80 to 90 µm separate grains in the matrix or as small inclusions (<20 µm) in garnet. They are mostly dark brown and have thin ilmenite overgrowth (Fig. 5b). Small zircons (<30 µm) are present either in garnet or the matrix. Some rutile grains have a retrograde rim of titanite and rutile enveloped by titanite (Fig. 5c). There is pseudomorphic replacement of garnet by chlorite-epidote assemblage (Fig. 5d). These textural features indicate gradual retrogression into greenschist-facies rocks.

4. Materials and Methods

4.1. Sample Preparation

Samples were prepared for trace element analysis as polished thin sections (quartz grains) of 50 µm (1184, 1202) and grain mounts (rutile grains; 1130, 1301). Photomicrographs were taken to identify the exact spots for laser ablation analysis and prepared for orientation using reflected light in the laser ablation sample cell. However, rutile grains from metagabbro (1130, 1301) were firstly concentrated by crushing, sieving, heavy liquid, magnetic separation and hand picking under a binocular microscope. These rutile grains were mounted in epoxy for trace element analysis and then polished. Transmitted and reflected light images were taken to define their position in the mount and polished thin sections. Backscattered electron (BSE) images were obtained using a Hitachi S-3400N scanning electron microscope (SEM) at the University of Gothenburg to identify inclusions in quartz-rutile grains and document the most suitable spots for analysis. The operating conditions during BSE imaging were maintained at 20 kV and 6.04 nA. Samples were cleaned by polishing with 1 µm alumina oxide powder to remove any carbon coating residual from SEM analysis. Then samples were put in an ultrasonic cleaning bath for 5 min and dried with ethanol-soaked tissue wiper to remove remaining surface contamination prior to being loaded into the laser ablation sample chamber.

10.57647/j.ijes.2025.16951

4.2. LA-ICPMS analysis

The in-situ trace element analyses of quartz and rutile grains were performed on polished thick sections and grain mounts at the Department of Earth Sciences at the University of Gothenburg. All samples were analysed using a New Wave NWR 213 laser ablation system coupled to an Agilent 8800 QQQ quadrupole ICP-MS. He-Ar mixture was used as carrier gas. Helium gas, which carries the laser-ablated sample aerosol from the sample cell, is mixed with argon carrier gas and nitrogen as additional di-atomic gas to enhance sensitivity, and finally flows into the ICPMS torch. Helium is flushed through the ablation cup at ~1 ml/min. Helium reduces surface deposition during ablation, which increases sensitivity and also reduces fractionation owing to particle size bias (Eggins et al., 1998).

Trace elements in rutile grains were analysed using a laser beam with diameter of 12 µm at laser energy of ~7.7 J/cm^2 and a repetition rate of 5 Hz. Signals were recorded over 60 s for each spot. The first 20 s were used to acquire background subtraction during laser warm-up. The following 30 s of dwell time were used for analysis of the sample by the ablation of rutile. The last 10 s were used for wash out. For trace element concentration in rutile, ^{27}Al, ^{51}V, ^{53}Cr, ^{57}Fe, ^{178}Hf, ^{181}Ta, ^{232}Th (10 ms dwell time), ^{49}Ti, ^{93}Nb (5 ms dwell time) and ^{90}Zr, ^{238}U (30 ms dwell time) were analysed. Each standard block is composed of two analyses of the R10 rutile standard and two analyses of NIST SRM 610 glass standard. Titanium, measured as ^{49}Ti, was used as internal standard element for all analyses. ^{90}Zr was used to determine the Zr concentration of rutile. The glass reference material NIST SRM 610 (Jochum and Nehring, 2006) and R10 (Luvizotto and Zack, 2009) rutile were used for external calibrations.

Trace elements in quartz grains were analysed using a laser beam with diameter of 50 µm at laser energy of ~30 J/cm^2 and a repetition rate of 4 Hz. Before analysing, polished thin sections were placed into the sample holder. Signals were recorded over 50 s for each spot. The first 10 s were used to acquire background subtraction during laser warm-up. The following 30 s of dwell time were used for analysis of quartz grains. The last 10 s were used for wash out. To analyse trace element concentration in quartz, ^{7}Li (9 ms dwell time), ^{23}Na (11 ms dwell time), ^{24}Mg, ^{27}Al, ^{28}Si, ^{48}Ti, ^{49}Ti (12 ms dwell time), ^{55}Mn, ^{56}Fe, ^{57}Fe, ^{71}Ga, ^{72}Ge (13 ms dwell time) were identified by the device. NIST SRM 610 glass standard (Jochum and Nehring, 2006) was used as primary standard. BCR-2G (natural basaltic glass standard) (Wilson, 1997) was used as secondary standard. These two standards were analysed after 10 spot analyses of quartz grains. ^{28}Si was used as internal standard element for all analyses. The concentrations of elements were determined using the "GLITTER version 4.4.4" software program (online interactive data reduction for LA-ICPMS microprobe (Van Achterbergh et al., 2000)). Ti and Si contents were initially assumed to be 100 wt % TiO_2 and SiO_2 during data reduction.

5. Results

5.1. Trace Element Composition of Rutile

Representative trace element concentrations of rutile grains are given in Table 1. Rutile occurs as three different textural types (matrix rutile, inclusion in garnet and inclusion in hornblende) in the studied samples. The most frequent type in samples (1184, 1202) is matrix rutile with a grain size between 80 and 90 µm (Fig. 5b). Rutile occurs as inclusions in garnet (grain size of rutile: 20 – 40 µm, Fig. 5c) and in hornblende (grain size of rutile: 10 – 20 µm, Fig. 5d). Moreover, larger crystals were separated from metagabbros (1130, 1301) with a grain size between 100 - 300 µm from intergrowths with ilmenite. Most porphyroblastic garnet grains exhibit small cracks containing retrograde minerals such as chlorite and epidote indicating possible pathways for trace element transfer during retrogression. Rutile from metagabbro (sample 1130) had Zr and Hf concentrations of 176 - 352 µg/g and 8-14 µg/g. The Nb and Ta contents varied from 180 to 363 µg/g and from 8 to 28 µg/g. The Zr and Hf concentrations of rutile from amphibolite (sample 1184) ranged between 289 and 428 µg/g and 10 and 18 µg/g, respectively, whereas Nb and Ta concentrations of sample 1184 varied between 748 and 811 µg/g and 39 and 49 µg/g. Rutile from amphibolite (sample 1202) had Zr and Hf contents of 250-302 µg/g and 9-11 µg/g, respectively. The Nb and Ta concentrations varied from 721 to 779 µg/g and from 62 to 73 µg/g. Rutile from metagabbro (sample 1301) had Zr and Hf contents of 176-399 µg/g and 8-15 µg/g, respectively. The Nb and Ta concentrations in rutile in this sample ranged from 125 to 336 µg/g and from 7 to 37 µg/g. V and Cr contents of rutile grains from metagabbro samples ranged from 704 to 1238 µg/g and 1131 to 3620 µg/g, respectively. However, a rutile grain from sample 1202 had the highest Fe concentration of 6816 µg/g.

BSE images of several rutile grains suggest the absence of systematic compositional zoning. Rutile grains were analysed at multiple spots, which usually had homogeneous Zr distribution (Fig. 6). However, in some places the rim is slightly enriched in Zr (Fig. 6a, b). Zr-rich phase separations are responsible for the variation of Zr concentrations in this rutile grain. Replacement by rutile of a pre-existing Zr-rich mineral like ilmenite is a

Table 1. LA-ICPMS trace element concentrations and estimated temperatures from rutile by Zr-in-rutile thermometry

Elements (μg/g) / Rock name (Sample no)	Grain no	V	Cr	Fe	W	Zr	Nb	Hf	Ta	Nb/Ta	Zr/Hf	T1	T2	T3	T4
Metagabbro (1130)	3	903	3162	1869	21	267	186	8	8	23	32	704	633	634	637
	3	903	2988	1655	19	268	180	9	9	20	30	704	633	634	637
	3	914	2854	1642	18	248	182	8	11	17	30	695	627	628	632
	3	927	2770	1885	29	254	191	8	11	17	31	698	629	630	633
	2	1013	2914	2013	41	305	218	10	11	19	30	721	644	645	647
	1	971	3282	1954	24	313	216	10	12	18	32	725	646	647	650
	5	1129	2349	2525	69	314	326	10	26	13	33	725	646	647	650
	4	843	2287	1433	21	287	212	14	11	19	20	713	639	640	643
	4	848	2282	2631	26	259	209	12	11	18	23	700	631	632	635
	4	876	2383	1710	24	299	224	12	12	19	26	718	642	643	646
	14	938	3472	2030	29	292	216	11	12	18	27	715	640	641	644
	14	940	3525	2729	27	302	202	10	11	18	30	720	643	644	647
	11	949	2688	2959	32	266	228	9	12	19	29	704	633	634	637
	10	957	2710	2294	25	286	234	10	14	16	27	713	639	640	642
	9	1238	2188	1662	51	176	363	8	28	13	23	651	601	602	606
	8	876	1777	1253	56	237	228	9	18	13	26	689	624	625	628
	13	919	2745	1376	17	285	120	9	8	15	32	712	638	639	642
	12	1069	1674	2182	20	274	223	8	18	12	33	707	635	636	639
	15	1027	3620	2017	36	352	200	12	14	14	30	739	656	656	659
											Avg	708	636	637	640
Amphibolite (1184)	21	1140	1167	2911	22	323	811	11	45	18	29	728	648	649	652
	22	793	2169	1485	212	289	765	12	49	16	24	714	639	640	643
	23	1126	1171	2525	10	428	748	18	40	19	24	764	672	673	675
	25	1297	1226	1041	33	357	796	10	41	19	36	741	657	658	660
	26	704	1892	1516	41	378	802	16	46	17	24	748	662	662	664
	27	817	1658	1467	30	391	759	10	40	19	39	753	665	665	667
	30	813	2140	1476	32	420	754	14	39	19	30	762	671	671	673
											Avg	745	659	660	662
Amphibolite (1202)	45	1104	3437	6816	85	302	779	11	73	11	27	720	643	644	647
	46	710	3355	2464	93	250	721	9	62	12	27	695	628	629	632
	47	926	2878	2620	66	278	748	10	64	12	28	709	636	637	640
	48	758	3216	2854	69	274	760	11	69	11	25	707	635	636	639
											Avg	708	635	636	639
Metagabbro (1301)	50	1213	1380	1784	25	381	176	13	8	22	30	750	662	663	665
	51	939	1444	2065	57	176	258	9	17	15	20	650	601	602	606
	52	959	2396	2883	31	333	336	14	18	19	23	732	651	652	654
	53	1191	1590	2099	103	301	248	10	18	14	30	719	643	644	646
	54	889	2932	2533	15	209	125	8	7	18	26	673	614	615	619
	55	836	1131	2820	19	340	226	15	18	13	23	735	653	654	656
	56	1119	1917	2158	44	236	210	10	10	21	24	689	623	625	628
	57	943	2368	2049	35	399	306	13	16	19	31	755	666	667	669
											Avg	717	641	642	643

1, 2, 3, 4 Temperatures were estimated according to thermometry of Zack et al., (2004), Watson et al., (2006), Ferry and Watson, (2007), and Tomkins et al., (2007) at 0.9 GPa, respectively.

10.57647/j.ijes.2025.16951

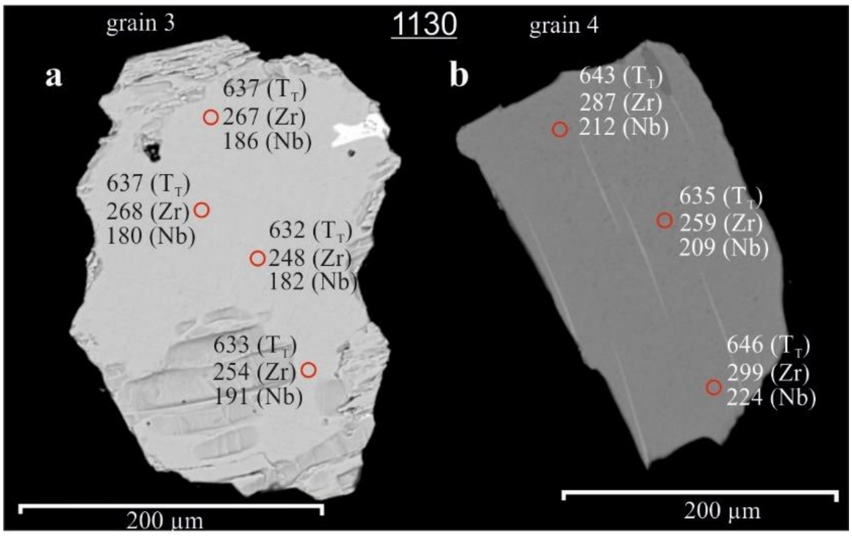

Figure 6. BSE images of rutile from sample 1130 (grain 3 and grain 4) used for multiple measurements. (a, b) Rutile grain with homogeneous Zr content throughout the grain but the rim is slightly enriched in Zr content. Circles mark the location of the spots analysed. The numbers give T_T (Tomkins et al., 2007) in ℃ and the contents of Zr and Nb in µg/g. Calculated temperatures vary from 636 to 651 ℃ indicating homogenous distribution of Zr-in-rutile

possible explanation for the formation of these Zr-rich phase separations in rutile (Austrheim et al., 2008; Meyer et al., 2011).

The concentrations and element ratios changes from sample to sample, which is more pronounced for Nb and Ta than Zr and Hf elements. Nb and Ta exhibit a strong positive correlation (Fig. 7a). Zr and Hf also indicate a positive correlation, but less distinct (Fig. 7b). Ta and Zr have negative correlation (1184), although three samples (1202, 1130, 1301) indicated a slight negative correlation (Fig. 7c).

5.2. Zr-in-Rutile Thermometer and Conventional Geothermobarometer

The average Zr concentrations and corresponding Zr-in-rutile temperatures are given in Table 1. The Zr contents of rutile grains ranged between 176 and 428 µg/g. Temperatures of rutile were calculated according to the Zr-in-rutile thermometry by Zack et al. (2004), Watson et al. (2006), Ferry and Watson, (2007) and Tomkins et al. (2007). The calibration of Zack et al. (2004) yielded temperatures of 708-745 ℃ with an average temperature of 720 ℃. These temperature estimations are higher than the temperatures estimated using other calibrations. Temperatures calculated by using the calibration of Watson et al. (2006) range between 635 and 659 ℃. This estimation has an average temperature of 643 ℃. The calibration of Ferry and Watson (2007) yielded temperatures of 636-660 ℃ with an average temperature of 644 ℃.

The temperatures of Watson et al. (2006) and Ferry and Watson (2007) are rather similar to each other. The Zr-in-rutile thermometer of Tomkins et al. (2007) is pressure dependent. The pressure value calculated by the conventional thermometers from the previous studies was used in this calibration. The garnet-biotite Fe–Mg exchange thermometer of Ferry and Spear (1978) gives temperatures of 640 to 690 ℃ (Okay and Satır, 2000). The widely used garnet-hornblende-plagioclase-quartz geobarometer (Kohn and Spear, 1990) yielded pressure of 0.9 GPa at a temperature of 660 ℃ (Okay and Satır, 2000; Şengün and Zack, 2016). Based on conventional geothermobarometers, a reasonable estimate for the peak P-T conditions in the meta-ophiolitic rocks is 0.9 GPa and 665±25 ℃ (Şengün and Zack, 2016). At 0.9 GPa, the Zr-in-rutile thermometer of Tomkins et al. (2007) gives 639-662 ℃ with an average temperature of 646 ℃.

5.3. TitaniQ Thermometer

Trace element analyses of quartz and temperatures estimated by the TitaniQ thermometer are given in Table 2. Ti contents of quartz from the sample 1184 ranged between 36 to 42 µg/g. However, Ti concentration in quartz from sample 1202 varied from 28 µg/g to 35 µg/g. Crystallization temperatures of quartz were calculated with the TitaniQ thermometer based on Ti contents of quartz. Rutile equilibrium and Ti activity in every phase were considered in this calibration. Quartz temperatures calculated by using the calibration of Wark and Watson (2006) range from 623 to 645 ℃ with an average temperature of 634 ℃. These temperatures give the crystallization temperatures of quartz. The calibration of Thomas et al. (2010) considers the pressure effect on Ti in quartz. Thus, the P-T conditions of ophiolitic metagabbros

10.57647/j.ijes.2025.16951

were constrained according to this calibration (Fig. 8, Thomas et al., 2010). Average Zr and Ti contents are 335 µg/g and 36 µg/g. Fig. 8 shows a P-T diagram for metagabbro samples with the range of Ti-in-quartz and Zr-in-rutile values plotted as isopleths. A P-T estimate can be obtained from the intersection of the Ti-in-quartz isopleths with the Zr-in-rutile isopleths, which yielded metamorphism conditions of ~660 ℃ and 1 GPa from this P-T diagram.

6. Discussion

6.1. Trace Element Characteristics of Rutile

Nb and Ta in rutile can dominate the whole rock Nb and Ta budget, and the average Nb/Ta ratio of rutile may be identical to that of the bulk rock. Rutile grains from all metagabbros have not only high HFSE contents, such as Nb (180-811 µg/g), Ta (8-73 µg/g), Zr (176-428 µg/g), Hf (8-18 µg/g), and W (10-103 µg/g),

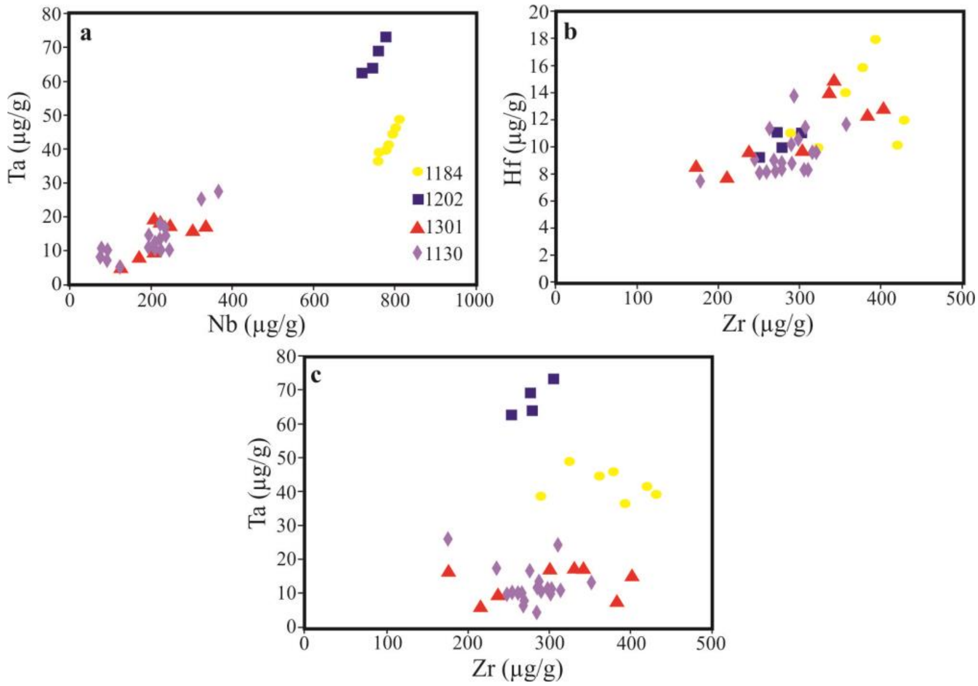

Figure 7. Results for HFSE concentrations in rutile from ophiolitic metagabbros in the Kazdağ Massif. Points refer to individual analyses. (a) Nb versus Ta indicating strong positive correlation. (b) Zr versus Hf also has positive correlation, but less distinctly. (c) Zr versus Ta showing slight negative correlation, except one sample (1202)

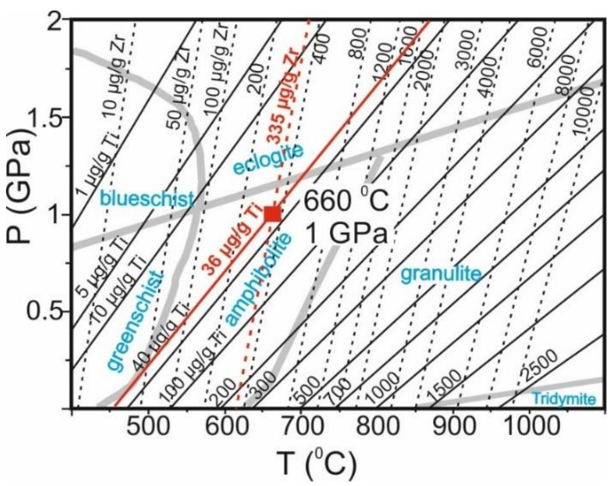

Figure 8. Ti-in-quartz and Zr-in-rutile isopleths used in this study as a thermobarometer for ophiolitic amphibolites in the Kazdağ Massif. Approximate metamorphic facies are generalized from Spear (1993) and Philpotts (1990)

Table 2. LA-ICPMS trace element concentrations and estimated temperatures of quartz by Ti-in-quartz thermometry

Element (µg/g)	Grain no	Li	Na	Mg	Al	Ti	Mn	Fe	T[1] (℃)
Rock name (Sample no)									
Amphibolite (1184)	114	5	22	20	27	41	1	16	650
	115	3	20	13	43	36	3	61	638
	116	5	9	16	46	38	1	7	643
	117	4	9	27	54	39	1	19	646
	118	3	12	12	31	40	1	4	648
	119	4	8	22	98	42	1	40	653
	120	4	14	28	26	38	1	32	643
	121	4	15	19	61	36	1	54	638
	122	3	8	14	50	39	1	22	646
								Ave	645
Amphibolite (1202)	122	4	9	7	78	30	1	90	621
	123	5	22	7	39	33	2	91	624
	124	5	11	2	67	32	1	60	627
	125	4	7	9	42	28	2	84	608
	126	5	8	6	47	34	3	51	633
	127	7	9	1	32	35	1	61	624
								Ave	623

[1] Temperatures were estimated by the calibration of Wark and Watson (2006)

but also high concentrations of transition metal elements such as V (704-1238 µg/g) and Cr (1131-3620 µg/g). Other trace elements have low concentrations or are below the detection limits. However, it is possible that the highest Fe content (6816 ppm) from one rutile grain (sample 1202) results from analysis of microscale mineral inclusions in the form of tiny ilmenite or iron oxide lamellae. Rutile grains from two amphibolite samples (1184, 1202) have high Nb and Ta concentrations, whereas rutile grains from two other samples (1130, 1301) include lower Nb and Ta concentrations (Table 1, Fig. 7a). It is likely that minerals with higher Ti contents have more influence on the behaviour of Nb and Ta owing to similar ionic radii and valence of Nb, Ta and Ti (Schmidt et al., 2004; Stepanov et al., 2013).

Nb/Ta ratios for rutile rims and cores are different from one another in one sample. The cores of rutile grains from sample 1130 are generally characterised by low Nb/Ta ratios of 17-18 whereas the rims exhibit relatively high Nb/Ta ratios of 19-23. The enrichment of Nb and Ta with slightly high Nb/Ta ratios in the rims of rutile may result from breakdown of hydrous minerals such as biotite (Zheng et al. 2011), which is equivalent to crystallization from a kind of geofluid that has a high content of water-insoluble trace elements (Zheng et al., 2011; Gao et al., 2014). Based on experimental data, the partition coefficients of Nb and Ta in rutile, usually displayed for any given rutile/melt pair, indicate D_{Nb} is always lower than D_{Ta} during the subduction processes (Schmidt et al., 2004; Klemme et al., 2005). If rutile was in equilibrium with such a melt, this could give rise to low Nb/Ta ratios in the initially grown rutile (Schmidt et al., 2009). Thus, the distinction of the behaviour of Nb/Ta fractionation specifies the compatibilities of Nb and Ta in rutile during rutile growth, which may be the basic outcome of Nb/Ta fractionation during metamorphic dehydration in subduction zones (Gao et al., 2014).

Trace element analyses in rutile suggest that these rutile grains grew from metamorphic fluids. Three types of geofluids occur in subduction zones, i.e., hydrous melt, aqueous solution and supercritical fluid, which have distinct capacities in dissolving and transporting trace elements (Hermann et al., 2006; Zheng et al., 2011). Generally, water-insoluble incompatible trace elements such as LREE and MREE can be dissolved and transported together with LILE by the hydrous melt;

10.57647/j.ijes.2025.16951

water-soluble incompatible trace elements such as LILE are mobile in the aqueous solution; and eventually all usually fluid-immobile incompatible trace elements such as HREE and HFSE can be dissolved and transported by supercritical fluid under subduction-zone amphibolite to high-pressure metamorphic conditions (e.g., Scambelluri et al., 2001; John et al., 2004; Hermann et al., 2006; Xia et al., 2010; Gao et al., 2014).

6.2. P-T conditions

The P-T conditions of meta-ophiolitic rocks in the Kazdağ Massif were estimated as 0.9 GPa and 665±25 °C by using conventional geothermobarometers (Şengün and Zack, 2016). Zr-in-rutile thermometry gives precise temperature estimates for meta-ophiolitic rocks in the Kazdağ Massif when compared to conventional thermometers. Four calibrations of the Zr-in-rutile thermometers were applied for temperature calculations (Zack et al., 2004; Watson et al., 2006; Ferry and Watson, 2007; Tomkins et al., 2007). All applied calibrations gave a similar temperature range except for the calibration of Zack et al. (2004) (Fig. 9), which is based on empirical and natural samples with the assemblage rutile-zircon-quartz. The Zr-in-rutile thermometer of Zack et al. (2004) gives the temperature range of 708-745 °C. This temperature range is higher than those calculated with the other calibrations (e.g., Miller et al., 2007; Baldwin et al., 2008; Meyer et al., 2011). The temperatures calculated by this calibration in this study confirm this observation and suggest that the recent experimental calibrations are more accurate than the empirical one. Subsequently, Watson et al. (2006), Ferry and Watson (2007) and Tomkins et al. (2007) improved the thermometer, resulting in more precise estimations over a wider temperature and pressure range. The calibration by Watson et al. (2006) is mainly based on experimental and natural results. The temperatures obtained using the Watson et al. (2006) calibration range between 635 and 659 °C. Ferry and Watson (2007) defined a silica activity factor in their experimental work. The Zr concentration in rutile is not only temperature-dependent, but also sensitive to the activity of SiO_2. The calibration of Ferry and Watson (2007) yielded temperatures of 636-660 °C. The experiments by both Watson et al. (2006) and Ferry and Watson (2007) were conducted at identical pressure of 1 GPa, which explains the mutually compatible results for these two calibrations. The 0.9 GPa calculated (Şengün and Zack, 2016) by conventional methods was used for meta-ophiolitic rocks, which experienced a lower pressure than ~1 GPa in these experimental calibrations. Therefore, the calibration by Tomkins et al. (2007) with a pressure correction is the best choice for temperature calculation. Furthermore, the calibration by Tomkins et al. (2007) is trustworthy for medium to high-grade metamorphic rocks, which gives more reliable temperatures than any other exchange thermometers (e.g., Spear et al., 2006; Miller et al., 2007; Luvizotto et al., 2009). Accordingly, the significance of a pressure correction should not be ignored for rocks which not only experienced more than 0.9 GPa pressure but also underwent metamorphism dominated by lower than 0.9 GPa pressure. The pressure used for metagabbro was assumed to be 0.9 GPa in the equation of Tomkins et al. (2007), based on a conventional geothermobarometer estimation of 0.9 GPa for the conditions of amphibolite-facies metamorphism. The Zr-in-rutile thermometer of Tomkins et al. (2007) gives temperatures of 639-662 °C

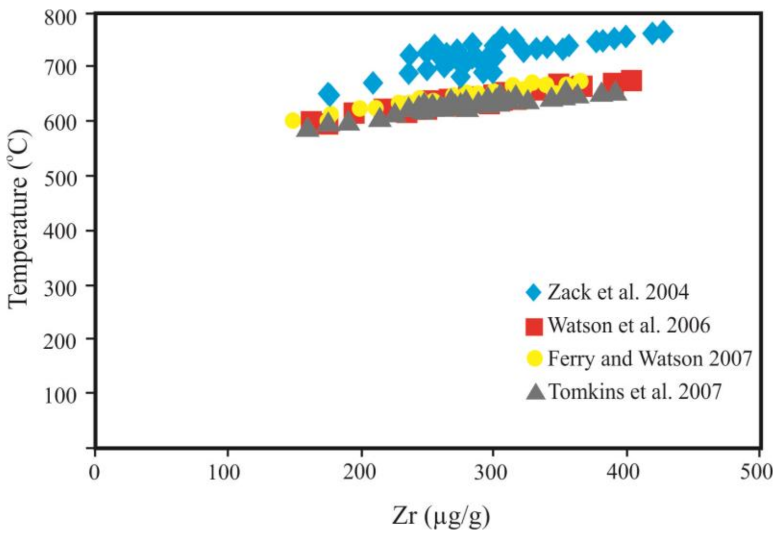

Figure 9. Difference in calculated temperature ranges from the Zr-in-rutile thermometer using various calibrations

10.57647/j.ijes.2025.16951

with an average temperature of 646 ℃ for metagabbro. Quartz and rutile are common in many metamorphic rocks. The pressure dependence of the TitaniQ thermometer makes it a potentially perfect barometer for ophiolitic metagabbros. The metagabbros contain rutile and quartz; thus, P-T dependencies of Ti-in-quartz can be combined with P-T dependencies of Zr-in-rutile to estimate pressure and temperature of crystallization for medium- to high-grade metamorphic rocks. P-dependency of the Ti-in-quartz thermometer makes it a trustworthy barometer for metagabbros, which gives more reliable pressure and temperature conditions. The P-T conditions of metagabbros were determined by Zr contents of rutile from the two rutile-bearing metagabbro samples (1130 and 1202) and Ti contents of quartz from the same samples. Ti in quartz and Zr in rutile values were plotted as isopleths on a P-T diagram (Fig. 8). If it is assumed that both quartz and the rutile crystals equilibrated at the peak of metamorphism, then the intersection of the isopleths yields the average P-T conditions of around 660 ℃ and 1 GPa. The P-T conditions estimated by using Ti-in-quartz thermobarometer are consistent with the previous Zr-in-rutile thermometer developed by Tomkins et al. (2007) and conventional geothermobarometers. The original TitaniQ calibration can be used to accurately determine quartz crystallization temperature for pressures near 1 GPa (Thomas et al., 2010). However, the P-T conditions of surrounding felsic gneisses were calculated by conventional thermometers. A reasonable estimate for the peak P-T conditions of medium- to high-grade metamorphic rocks in the Kazdağ Massif is 0.5±0.1 GPa and 640±50 ℃ (Okay and Satır, 2000). These P-T conditions show that metamorphic rocks exposed in the Kazdağ Massif experienced amphibolite-facies metamorphism. On the other hand, the estimated pressure value for metagabbros is higher than the estimated pressure value for surrounding felsic gneisses. This suggests that the meta-ophiolitic rocks occur as a different tectonic slice in the Kazdağ Massif and underwent amphibolite-facies metamorphism at ~35 km according to pressure estimations, whereas the metamorphic rocks of the Kazdağ Massif underwent amphibolite-facies metamorphism at ~20 km. Metamorphism resulted from northward subduction of the İzmir-Ankara branch of the Neo-Tethyan Ocean under the Sakarya Zone. Following metamorphism, the medium- to high-grade metamorphic rocks of the Kazdağ Massif were internally imbricated by southerly compression during collision. When evaluated from a tectonic point of view, the Kazdağ metamorphic sequence was imbricated along thrust faults with southward vergence after Alpine metamorphism (Erdoğan et al., 2013) and meta-ophiolitic rocks were emplaced as a different tectonic slice. Collision of the Sakarya Zone with the Anatolide-Tauride Block and internal imbrications of the Kazdağ Massif gave rise to progressive thickening in the crust.

7. Conclusions

Meta-ophiolitic rocks are exposed in the Kazdağ Massif located in the northwestern part of Anatolia. The Nb/Ta and Zr/Hf ratios increase with a decrease in Ta and Hf contents, which could be ascribed to the effect of metamorphic dehydration with rutile Nb/Ta differentiation. Trace element analyses in rutile suggest that these rutile grains grew from metamorphic fluids. An aqueous solution with high Nb/Ta ratios can be derived from metamorphic dehydration due to the breakdown of biotite during the exhumation of subducted oceanic crust. Rutile rims are rich in Nb and Ta which results in slightly high Nb/Ta ratios. The enrichment of Nb and Ta in rutile rims suggests local enrichment of these water-insoluble incompatible trace elements in metamorphic fluid.

Ti-in-quartz and Zr-in-rutile thermometers were applied to quartz-zircon-rutile-bearing amphibolites to estimate pressure and temperature of meta-ophiolitic rocks in the Kazdağ Massif. Four calibrations of the Zr-in-rutile thermometer were applied for temperature calculations. The calibration of Tomkins et al. (2007) with a pressure correction is the best choice for temperature calculations. The Zr-in-rutile thermometer of Tomkins et al. (2007) yields temperatures of 639-662 ℃ (average 646 ℃) at 0.9 GPa for meta-ophiolitic rocks in the Kazdağ Massif, which reflects the metamorphic temperature. The pressure value calculated by conventional geothermobarometers was used for temperature estimations in this calibration. The P-T dependence of Ti-in-quartz was combined with P-T dependence of Zr-in-rutile to estimate pressure and temperature of crystallization. A P-T estimate can be obtained from the intersection of the Ti-in-quartz isopleths with the Zr-in-rutile isopleths, which yielded metamorphism conditions of ~660 ℃ and 1 GPa. TitaniQ thermobarometer is a trustworthy thermobarometer for medium- to high-grade metamorphic rocks, which gives more reliable pressure and temperature. The P-T conditions of meta-ophiolitic rocks suggest that the meta-ophiolitic rocks occur as a different tectonic slice in the Kazdağ metamorphic sequence and underwent amphibolite-facies metamorphism at ~35 km. Metamorphism took place due to the northward subduction of the İzmir-Ankara branch of the Neo-Tethyan Ocean under the Sakarya Zone. The northward subduction of the İzmir-Ankara branch of the Neo-Tethyan Ocean under the Sakarya Zone was accompanied by N-S contraction during which the regionally metamorphosed Kazdağ Massif was internally imbricated.

10.57647/j.ijes.2025.16951

This imbrication is possibly the main reason for thickening and exhumation of the Kazdağ Massif.

Acknowledgments

This study was supported by the Scientific Research Coordination Unit of Çanakkale Onsekiz Mart University with project number of FHD-2024–4690. I warmly thank Thomas Zack for his help with the LA-ICPMS measurements in Gothenburg University.

Authors Contribution
All the authors have participated sufficiently in the intellectual content, conception, and design of this work or the analysis and interpretation of the data (when applicable), as well as the writing of the manuscript.

Availability of data and materials
The data that support the findings of this study are available from the corresponding author upon reasonable request.

Conflict of interest
The author states that there is no conflict of interest.

References

Ashrafi, N., Dabiri, R., & Jahangiri, A. (2024) Some chemical variations in biotite, phlogopite, and muscovite, considering their tectonic setting, *Geopersia*, *14*(2), 307-325. https://doi.org/10.22059/geope.2024.373882.648749

Austrheim, H., Putnis, C. V., Engvik, A. K., & Putnis, A. (2008). Zircon coronas around Fe-Ti oxides: A physical reference frame for metamorphic and metasomatic reactions. *Contribution to Mineralogy and Petrology, 156*, 517–527. https://doi.org/10.1007/s00410-008-0299-8

Aysal, N., Ustaömer, T., Öngen, S., Keskin, M., Köksal, S., Peytcheva, I., & Fanning, M. (2012). Origin of the Early-Middle Devonian magmatism in the Sakarya Zone, NW Türkiye: Geochronology, geochemistry, and isotope systematics. *Journal of Asian Earth Sciences, 45*, 201–222. https://doi.org/10.1016/j.jseaes.2011.10.011

Baldwin, J. A., & Brown, M. (2008). Age and duration of ultrahigh-temperature metamorphism in the Anápolis Itauçu Complex, Southern Brasília Belt, central Brazil – Constraints from U-Pb geochronology, mineral rare earth element chemistry and trace element thermometry. *Journal of Metamorphic Geology, 26*, 213–233. https://doi.org/10.1111/j.1525-1314.2007.00759.x

Beccaletto, L., & Jenny, C. (2004). Geology and correlation of the Ezine Zone: A Rhodope fragment in NW Türkiye? *Turkish Journal of Earth Science, 13*, 145–176.

Bingöl, E. (1969). Central of the Kazdağ Massif and geology of the southeastern part. *Bulletin of the Mineral Research and Exploration, 72*, 110–123.

Bingöl, E., Akyürek, B., & Korkmazer, B. (1975). Geology of the Biga Peninsula and some features of the Karakaya Complex. In *50th Anniversary Geological Congress, Abstracts* (pp. 70–76). MTA.

Borojenie, T. H., Sheykhzakariaei, S. J., Dabiri, R., & Yazdi, A. (2025). Petrogenesis and tectonic implications of Neoproterozoic to Cenozoic A-type granitoids in NW Iran: Geochemical and tectonic constraints. *Iranian Journal of Earth Sciences, 17*(4), 1–19. https://doi.org/10.57647/j.ijes.2025.16894

Brenan, J. M., Shaw, H. F., Phinney, D. L., & Ryerson, F. J. (1994). Rutile-aqueous fluid partitioning of Nb, Ta, Hf, Zr, U and Th: Implications for high field strength element depletions in island-arc basalts. *Earth and Planetary Science Letters, 128*, 327–339. https://doi.org/10.1016/0012-821X(94)90154-6

Cavazza, W., Okay, A. I., & Zattin, M. (2009). Rapid early-middle exhumation of the Kazdağ Massif (western Anatolia). *International Journal of Earth Sciences, 98*, 1935–1947. https://doi.org/10.1007/s00531-008-0353-9

Deer, W. A., Howie, R. A., & Zussman, J. (1992). *An Introduction to Rock-Forming Minerals*. Longman Group.

Ding, X., Hu, Y. H., Zhang, H., Li, C. Y., Ling, M. X., & Sun, W. D. (2013). Major Nb/Ta fractionation recorded in garnet amphibolite facies metagabbro. *Journal of Geology, 121*, 255–274. https://doi.org/10.1086/669978

Dürr, S., Alther, R., Keller, J., Okrusch, M., & Seidel, E. (1978). The median Aegean crystalline belt: Stratigraphy, structure, metamorphism, magmatism. In H. Closs, D. Roeder, & K. Schmidt (Eds.), *Alps, Appenines and Hellenides* (pp. 455–476). Scheweizerbart.

Duru, M., Pehlivan, Ş., Şentürk, Y., Yavaş, F., & Kar, H. (2004). New results on the lithostratigraphy of the Kazdağ Massif in Northwest Türkiye. *Turkish Journal of Earth Science, 13*, 177–186.

Eggins, S., Kinsley, L., & Shelley, J. (1998). Deposition and element fractionation processes during atmospheric pressure laser sampling for analysis by ICP-MS. *Applied Surface Science, 127*, 278–286. https://doi.org/10.1016/S0169-4332(97)00643-0

Erdoğan, B., Akay, E., Hasözbek, A., Satır, M., & Siebel, W. (2013). Stratigraphy and tectonic evolution of the Kazdağ Masif (NW Anatolia) based on field studies and radiometric ages. *International Geology Review, 55*(17), 2060–2082. https://doi.org/10.1080/00206814.2013.818756

Ewing, T. A., Herman, J., & Rubatto, D. (2013). The robustness of the Zr-in-rutile and Ti-in-zircon thermometers during high-temperature metamorphism (Ivrea-Verbano zone, northern Italy). *Contribution to Mineralogy and Petrology, 165*(4), 757–779. https://doi.org/10.1007/s00410-012-0834-5

Ferry, J. M., & Spear, F. S. (1978). Experimental calibration of the partitioning of Fe and Mg between biotite and garnet. *Contribution to Mineralogy and Petrology, 66*(1), 113–117. https://doi.org/10.1007/BF00372150

Ferry, J. M., & Watson, E. B. (2007). New thermodynamic models and revised calibrations for the Ti-in-zircon and Zr-in-rutile thermometers. *Contribution to Mineralogy and Petrology, 154*(4), 429–437. https://doi.org/10.1007/s00410-007-0201-0

Foley, S., Tiepolo, M., & Vannucci, R. (2002). Growth of early continental crust controlled by melting of amphibolite in subduction zones. *Nature, 417*(6891), 837–840. https://doi.org/10.1038/nature00799

Foley, S. F., Barth, M. G., & Jenner, G. A. (2000). Rutile/melt partition coefficients for trace elements and assessment of the influence of rutile on the trace element characteristics of subduction zone magmas. *Geochimica et Cosmochimica Acta, 64*(6), 933–938. https://doi.org/10.1016/S0016-7037(99)00355-5

Gao, X. Y., Zheng, F. Y., Xia, X. P., & Chen, Y. P. (2014). U-Pb ages and trace element of metamorphic rutile from ultrahigh-pressure quartzite in the Sulu orogen. *Geochimica et Cosmochimica Acta, 143*, 87–114. https://doi.org/10.1016/j.gca.2014.04.032

Graham, J., & Morris, R. C. (1973). Tungsten- and antimony substituted rutile. *Mineralogical Magazine, 39*(304), 470–473. https://doi.org/10.1180/minmag.1973.039.304.11

Green, T. H. (1995). Significance of Nb/Ta as an indicator of geochemical processes in the crust–mantle system. *Chemical Geology, 120*(3-4), 347–359. https://doi.org/10.1016/0009-2541(94)00145-X

Hermann, J., Spandler, C., Hack, A., & Korsakov, A. (2006). Aqueous fluids and hydrous melts in high-pressure and ultra-high-pressure rocks: Implications for element transfer in subduction zones. *Lithos, 92*(1-2), 399–417. https://doi.org/10.1016/j.lithos.2006.03.055

Jochum, K. P., & Nehring, F. (2006). NIST 610: GeoReM preferred values (11/2006). *GeoReM*. http://georem.mpch-mainz.gwdg.de

John, T., Scherer, E. E., Haase, K., & Schenk, V. (2004). Trace element fractionation during fluid-induced eclogitization in a subducting slab: trace element and Lu-Hf-Sm-Nd isotope systematics. *Earth and Planetary Science Letters, 227*(3-4), 441–456. https://doi.org/10.1016/j.epsl.2004.09.009

Karslı, O., Şengün, F., Dokuz, A., Kandemir, R., Aydin, F., & Andersen, T. (2020). Silurian to Early Devonian arc magmatism in the western Sakarya Zone (NW Türkiye), with inference to the closure of the Rheic Ocean. *Lithos, 370-371*, 105641. https://doi.org/10.1016/j.lithos.2020.105641

Klemme, S., Prowatke, S., Hametner, K., & Gunther, D. (2005). Partitioning of trace elements between rutile and silicate melts: Implications for subduction zones. *Geochimica et Cosmochimica Acta, 69*(10), 2361–2371. https://doi.org/10.1016/j.gca.2004.11.015

Kohn, M. J., & Spear, F. S. (1990). Two new geobarometers for garnet amphibolite so with applications to southeastern Vermont. *American Mineralogist, 75*(1-2), 89–96.

Luvizotto, G. L., & Zack, T. (2009). Nb and Zr behavior in rutile during high-grade metamorphism and retrogression: An example from the Ivrea–Verbano Zone. *Chemical Geology, 261*(3-4), 303–317. https://doi.org/10.1016/j.chemgeo.2008.07.023

Meinhold, G. (2010). Rutile and its applications in earth sciences. *Earth Science Reviews, 102*(1-2), 1–28. https://doi.org/10.1016/j.earscirev.2010.06.001

Meinhold, G., Kostopoulos, D., Frei, D., Himmerkus, F., & Reischmann, T. (2010). U-Pb LA-SF ICP-MS zircon geochronology of the Serbo-Macedonian Massif, Greece: Palaeotectonic constraints for Gondwana-derived terranes in the Eastern Mediterranean. *International Journal of Earth Sciences, 99*(5), 813–832. https://doi.org/10.1007/s00531-009-0425-5

Meyer, M., John, T., Brandt, S., & Klemd, R. (2011). Trace element composition of rutile and the application of Zr-in-rutile thermometry to UHT metamorphism (Epupa Complex, NW Namibia). *Lithos, 126*(1-4), 388–401. https://doi.org/10.1016/j.lithos.2011.07.013

Miller, C., Zanetti, A., & Thoni, M. (2007). Eclogitisation of gabbroic rocks: Redistribution of trace elements and Zr in rutile thermometry in an Eo-Alpine subduction zone (Eastern Alps). *Chemical Geology, 239*(1-2), 96–123. https://doi.org/10.1016/j.chemgeo.2007.01.001

Moix, P., Beccaletto, L., Kozur, H., Hochard, C., Rosselet, F., & Stampfli, G. M. (2008). A new classification of the Turkish terranes and sutures and its implication for the palaeotectonic history of the region. *Tectonophysics, 451*(1-4), 7–39. https://doi.org/10.1016/j.tecto.2007.11.044

Mollai, H., Dabiri, R., Torshizian, H. A., Pe-Piper, G., & Wang, W. E. (2021). Upper Neoproterozoic garnet-bearing granites in the Zeber-Kuh region from east central Iran micro plate: Implications for the magmatic evolution in the northern margin of Gondwanaland. *Geologica Carpathica, 72*(6), 461–481. http://dx.doi.org/10.31577/GeolCarp.72.6.2

MTA. (2012). *General and economic geology of the Biga Peninsula* (Special Publication Series 28).

Nazari, M., Arian, M. A., Solgi, A., Zareisahamieh, R., & Yazdi, A. (2023). Geochemistry and tectonomagmatic environment of Eocene volcanic rocks in the Southeastern region of Abhar, NW Iran. *Iranian Journal of Earth Sciences, 15*(4), 228–247. https://doi.org/10.30495/ijes.2023.1956689.1746

Okay, A. I. (1984). Distribution and characteristics of the northwest Turkish blueschists. In A. H. F. Robertson & J. E. Dixon (Eds.), *The geological evolution of the eastern Mediterranean* (pp. 455–466). Geological Society of London Special Publications 17. https://doi.org/10.1144/GSL.SP.1984.017.01.33

Okay, A. I. (1986). High-pressure/low-temperature metamorphic rocks of Türkiye. *Memoirs of the Geological Society of America, 164*, 333–347. https://doi.org/10.1130/MEM164-p333

Okay, A. İ., & Göncüoğlu, M. C. (2004). The Karakaya Complex: A Review of Data and Concepts. *Turkish Journal of Earth Sciences, 13*, 77–95.

Okay, A. I., & Satır, M. (2000). Coeval plutonism and metamorphism in a latest Oligocene metamorphic core complex in Northwest Türkiye. *Geological Magazine, 137*(5), 495–516. https://doi.org/10.1017/S0016756800004532

Okay, A. I., Satır, M., Maluski, H., Siyako, M., Monie, P., Metzger, R., & Akyüz, S. (1996). Paleo and Neotethyan events in northwest Türkiye. In A. Yin & M. Harrison (Eds.), *Tectonics of Asia* (pp. 420–441). Cambridge University Press.

Okay, A. I., Satir, M., & Siebel, W. (2006). Pre-Alpide and Mesozoic orogenic events in the Eastern Mediterranean region. *Geological Society of Special Publications 32*, 389–405. https://doi.org/10.1144/GSL.MEM.2006.032.01.23

Okay, A. I., Siyako, M., & Bürkan, K. A. (1991). Geology and tectonic evolution of the Biga Peninsula. *Bulletin of the Technical University of Istanbul, 44*, 191–255.

Okay, A. I., & Topuz, G. (2017). Variscan orogeny in the Black Sea region. *International Journal of Earth Sciences, 106*, 569–592. https://doi.org/10.1007/s00531-016-1395-z

Okay, A. I., & Tüysüz, O. (1999). Tethyan sutures of northern Türkiye. In B. Durand, L. Jolivet, F. Horváth, & M. Séranne (Eds.), *The Mediterranean Basins: Tertiary Extension within the Alpine*

Orogen (pp. 475–515). Geological Society of Special Publications 156. https://doi.org/10.1144/GSL.SP.1999.156.01.22

Philpotts, A. R. (1990). *Principles of igneous and metamorphic petrology*. Prentice Hall.

Rudnick, R. L., Barth, M., Horn, I., & McDonough, W. F. (2000). Rutile-bearing refractory eclogites: missing link between continents and depleted mantle. *Science, 287*(5451), 278–281. https://doi.org/10.1126/science.287.5451.278

Salehpour, S., Arian, M. A., Rad, A. J., Zarei Sahamieh, R., & Yazdi, A. (2025). Geochemistry and technomagmatic environment of Eocene volcanic rocks in Yuzbashi Chay region, west of Qazvin (Iran). *Iranian Journal of Earth Sciences, 17*(1), 1–13. https://doi.org/10.57647/j.ijes.2025.1701.04

Scambelluri, M., Bottazzi, P., Trommsdorff, V., Vannucci, R., Hermann, J., Gomez-Pugnaire, M. T., & Lopez-Sanchez-Vizcaino, V. (2001). Incompatible element-rich fluids released by antigorite breakdown in deeply subducted mantle. *Earth and Planetary Science Letters, 192*, 457–470. https://doi.org/10.1016/S0012-821X(01)00457-5

Schmidt, A., Weyer, S., John, T., & Brey, G. P. (2009). HFSE systematics of rutile-bearing eclogites: new insights into subduction zone processes and implications for the earth's HFSE budget. *Geochimica et Cosmochimica Acta, 73*(2), 455–468. https://doi.org/10.1016/j.gca.2008.10.028

Schmidt, M. W., Dardon, A., Chazot, G., & Vannucci, R. (2004). The dependence of Nb and Ta rutile–melt partitioning on melt composition and Nb/Ta fractionation during subduction processes. *Earth and Planetary Science Letters, 226*(3-4), 415–432. https://doi.org/10.1016/j.epsl.2004.08.010

Şengör, A. M. C., & Yılmaz, Y. (1981). Tethyan evolution of Türkiye: A plate tectonic approach. *Tectonophysics, 75*(3-4), 181–241. https://doi.org/10.1016/0040-1951(81)90275-4

Şengün, F., Yigitbas, E., & Tunç, İ. O. (2011). Geology and Tectonic Emplacement of Eclogite and Blueschist, Biga Peninsula, Northwest Türkiye. *Turkish Journal of Earth Science, 20*(4), 273–285. https://doi.org/10.3906/yer-0912-75

Şengün, F., & Zack, T. (2016). Trace element composition of rutile and Zr-in-rutile thermometry in meta-ophiolitic rocks from the Kazdağ Massif, NW Türkiye. *Mineralogy and Petrology, 110*(3), 547–560. https://doi.org/10.1007/s00710-016-0433-7

Şengün, F., Hasözbek, A., & Doğan-Külahcı, G. D. (2023). The geochemistry, origin and tectonic setting of the Tozlu metaophiolite in the Kazdağ Massif (Biga Peninsula, NW Anatolia). *Geologica Carpathica, 74*(4), 281–296. https://doi.org/10.31577/GeolCarp.2023.16

Spear, F. S. (1993). *Metamorphic phase equilibria and pressure-temperature-time paths*. Mineralogical Society of America.

Spear, F. S., Wark, D. A., & Cheney, J. T. (2006). Zr-in-rutile thermometry in blueschists from Sifnos, Greece. *Contribution to Mineralogy and Petrology, 152*(3), 375–385. https://doi.org/10.1007/s00410-006-0113-4

Stepanov, A. S., & Hermann, J. (2013). Fractionation of Nb and Ta by biotite and phengite: implications for the "missing Nb paradox". *Geology, 41*(3), 303–306. https://doi.org/10.1130/G33781.1

Thomas, J. B., Watson, E. B., Spear, F. S., Shemella, F. S., Nayak, S. K., & Lanzirotti, A. (2010). TitaniQ under pressure: the effect of pressure and temperature on the solubility of Ti in quartz. *Contribution to Mineralogy and Petrology, 160*(5), 743–759. https://doi.org/10.1007/s00410-010-0505-3

Thomas, J. B., Watson, E. B., Spear, F. S., & Wark, D. A. (2015). TitaniQ recrystallized: experimental confirmation of the original Ti in quartz calibrations. *Contribution to Mineralogy and Petrology, 169*(1), 27. https://doi.org/10.1007/s00410-015-1120-0

Tomkins, H. S., Powell, R., & Ellis, D. J. (2007). The pressure dependence of the zirconium-in-rutile thermometer. *Journal of Metamorphic Geology, 25*(6), 703–713. https://doi.org/10.1111/j.1525-1314.2007.00724.x

Topuz, G., Candan, O., Okay, A. I., von Quad, A., Othman, M., Zack, T., & Wang, J. (2020). Silurian anorogenic basic and acidic magmatism in Northwest Türkiye: Implications for the opening of the Paleo-Tethys. *Lithos, 356-357*, 105302. https://doi.org/10.1016/j.lithos.2019.105302

Van Achterbergh, E., Ryan, C. G., & Griffin, W. L. (2000). *GLITTER (Version 3.0, On-line Interactive Data Reduction for LA-ICPMS)*. Maquarie Research Ltd.

Wark, D. A., & Watson, E. B. (2006). The TitaniQ: a Titanium-in-quartz geothermometer. *Contribution to Mineralogy and Petrology, 152*(4), 743–754. https://doi.org/10.1007/s00410-006-0132-1

Warr, L. (2021). IMA-CNMNC approved mineral symbols. *Mineralogical Magazine, 85*(3), 291–320. https://doi.org/10.1180/mgm.2021.43

Watson, E. B., Wark, D. A., & Thomas, J. B. (2006). Crystallization thermometers for zircon and rutile. *Contribution to Mineralogy and Petrology, 151*(4), 413–433. https://doi.org/10.1007/s00410-006-0068-5

Wilson, S. A. (1997). *The collection, preparation, and testing of USGS reference material BCR-2, Columbia River, Basalt* (Open-File Report 98). U.S. Geological Survey.

Xia, Q. X., Zheng, Y. F., & Hu, Z. C. (2010). Trace elements in zircon and coexisting minerals from low-T/UHP metagranite in the Dabie orogen: implications for action of supercritical fluid during continental subduction-zone metamorphism. *Lithos, 114*(3-4), 385–412. https://doi.org/10.1016/j.lithos.2009.09.013

Yazdi, A., Ashja-Ardalan, A., Emami, M. H., Dabiri, R., & Foudazi, M. (2017). Chemistry of Minerals and Geothermobarometry of Volcanic Rocks in the Region Located in Southeast of Bam, Kerman Province. *Open Journal of Geology, 7*(11), 1644–1653. https://doi.org/10.4236/ojg.2017.711110

Yiğitbaş, E., Şengün, F., & Tunç, İ. O. (2014). *Pre-Neogene tectonic units in the Biga Peninsula and an approach to geodynamic evolution of region*. (TUBITAK Project 110Y281).

Zack, T., Kronz, A., Foley, S. F., & Rivers, T. (2002). Trace element abundances in rutiles from eclogites and associated garnet mica schists. *Chemical Geology, 184*(1-2), 97–122. https://doi.org/10.1016/S0009-2541(01)00357-6

Zack, T., & Luvizotto, G. L. (2006). Application of rutile thermometry to eclogites. *Mineralogy and Petrology, 88*(1-2), 69–85. https://doi.org/10.1007/s00710-006-0145-5

Zack, T., Moraes, R., & Kronz, A. (2004). Temperature dependence of Zr in rutile: empirical calibration of a rutile thermometer. *Contribution to Mineralogy and Petrology, 148*(4), 471–488. https://doi.org/10.1007/s00410-004-0617-8

Zhang, J. X., Yu, S., Meng, F. C., & Li, J. P. (2009). Paired high-pressure granulite and eclogite in collision orogens and their geodynamic implications. *Acta Petrologica Sinica, 25*(9), 2050–2066.

Zheng, Y. F., Xia, Q. X., Chen, R. X., & Gao, X. Y. (2011). Partial melting, fluid supercriticality and element mobility in ultrahigh-pressure metamorphic rocks during continental collision. *Earth Science Reviews, 107*(3-4), 342–374. https://doi.org/10.1016/j.earscirev.2011.04.004